applied sciences

MDPI

Article

Ammonia/Ethane Blends Combustion and Oxidation: Experimental and Numerical Study

Ksenia N. Osipova [1], Vladislav V. Matyushkov [1], Alexander V. Drakon [2], Stanislav A. Trubachev [1] and Andrey G. Shmakov [1,*]

[1] Voevodsky Institute of Chemical Kinetics and Combustion SB RAS, Novosibirsk 630090, Russia; osipova@kinetics.nsc.ru (K.N.O.); mvv@kinetics.nsc.ru (V.V.M.); trubachev@kinetics.nsc.ru (S.A.T.)
[2] Joint Institute for High Temperatures RAS, Moscow 125412, Russia; drakon.a.v@gmail.com
* Correspondence: shmakov@kinetics.nsc.ru

Featured Application

This study aims to address the scarcity of experimental data on the combustion of ammonia/ethane mixtures. It presents measurements of flame structure, ignition delay times, and speciation in JSR for various ammonia/ethane blends under a wide range of conditions. The flame structure of these mixtures is investigated for the first time at both atmospheric and elevated pressures, simulating conditions relevant to engine combustion chambers. These new data, combined with ignition delay times obtained in a shock tube and oxidation data from the JSR, enable a comprehensive evaluation of published mechanisms for ammonia–ethane combustion. The experimental data are used to assess the predictive capability of 11 detailed published kinetic models. Overall, this significantly extends the experimental database for the oxidation of ammonia/hydrocarbon mixtures, contributing to the refinement of chemical kinetic models. This, in turn, offers the prospects for the large-scale use of ammonia-based mixtures as alternative fuels.

Abstract

Ammonia is considered as a promising hydrogen carrier and a carbon-free fuel. Methods for improving ammonia combustion characteristics often involve its co-firing with more reactive fuels (natural gas, biofuels, etc.). Among the natural gas components, ethane is second most abundant. Therefore, the development of detailed chemical–kinetic mechanisms that accurately consider the interactions between ammonia and each component of natural gas is very important. Such mechanisms must be based on experimental data obtained under a wide range of conditions. In this work, $NH_3/C_2H_6/O_2/Ar$ blends were studied in JSR (φ = 0.5–2.0, p = 1 atm, τ = 1 s, T = 800–1300 K) and in a shock tube (p = 7.3–8.6 atm, T = 1260–1590 K). Additionally, the structure of premixed flames was investigated (φ = 0.8–1.2, p = 1–5 atm). Eleven recently published detailed chemical–kinetic mechanisms were tested. The model Shrestha-2025 was updated to achieve better agreement with the entire set of experimental data. The effect of p and φ on intermediate species concentration was analyzed. Ammonia and ethane consumption pathways were also examined.

Keywords: ammonia; ethane; jet-stirred reactor; molecular beam mass spectrometry; shock tube; chemical kinetic mechanism

Check for updates

Academic Editor: Janusz Lasek

Received: 8 December 2025
Revised: 3 January 2026
Accepted: 7 January 2026
Published: 8 January 2026

Copyright: © 2026 by the authors. Licensee MDPI, Basel, Switzerland. This article is an open access article distributed under the terms and conditions of the Creative Commons Attribution (CC BY) license.

1. Introduction

Recently, ammonia has attracted attention as a promising hydrogen carrier and a potential carbon-free fuel. Ammonia utilization would reduce emissions of carbon-containing species, which is important from an environmental standpoint. However, pure ammonia is unsuitable for practical applications as a standalone fuel. This is due to its low burning velocity and inevitably high NOx emissions resulting from the fuel nitrogen. One possible solution is the co-firing of ammonia with hydrogen or carbon-containing fuels (e.g., natural gas, diesel, etc.). Consequently, there is a need to develop reliable detailed chemical–kinetic mechanisms of combustion and oxidation for ammonia–hydrocarbon blends. While oxygenates are also considered as potential pilot fuels for ammonia, C_1-C_4 hydrocarbons offer several advantages due to their higher heat of combustion and gaseous state at atmospheric pressure. Oxygenates, having a lower heat of combustion, must be added in larger fractions to achieve a heating effect equivalent to that of NH_3/C_1-C_4 mixtures. If one disregards the potential for producing oxygenates from renewable bioresources, the advantage in terms of reducing CO_2 emissions becomes negligible. Furthermore, most oxygenates, except dimethyl ether, are liquids at normal pressure, necessitating a more complex fuel preparation system compared to mixtures of NH_3 with gaseous C_1-C_4 hydrocarbons.

Natural gas, one of the most widespread and inexpensive energy sources, can contain a significant amount of ethane. Its concentration, depending on the specific deposit, can reach approximately 4–8% [1]. Furthermore, ethane is a key intermediate formed during the oxidation of heavier hydrocarbons and can therefore interact with nitrogen-containing compounds in a flame. These two aspects support the importance of studying such systems.

However, a literature review shows that, compared to ammonia/hydrogen and ammonia/methane mixtures, the number of studies focused on the combustion and oxidation of ammonia/ethane blends is extremely limited. The main information about these works is summarized in Table 1. A more detailed description is provided below.

Table 1. The works focused on the study of ammonia/ethane blends' combustion and oxidation.

Measured Parameters	Method	Blend Composition	NH_3/C_2H_6 Molar Ratio	T (K)	*p* (atm)	φ	Ref
IDT	ST	$NH_3/C_2H_6/O_2/N_2$	2.4:1–10:1	1200–1800	1	1.0	[1]
IDT	ST	$NH_3/CH_4/C_2H_6/C_3H_8/O_2/Ar$	-	1450–1900	10	1.0	[2]
IDT	RCM	$NH_3/C_2H_6/O_2/Ar/N_2$	9:1–99:1	890–1110	20 and 40	0.5–2.0	[3]
IDT	ST	$NH_3/C_2H_6/O_2/Ar$	9:1–2.3:1	1227–1890	1.75 and 10	1.0	[4]
IDT, SP	ST	$NH_3/C_2H_6/O_2/Ar$	18.6:1–9:1–4:1	1317–1957	~2.8	0.5/1.0/1.5	[5]
LBV	CVCC	NH_3/C_2H_6/air	1:0–0:1	298	1	1.0	[6]
LBV	HF	NH_3/C_2H_6/air	9:1–1:1–0:1	298	1	0.6–1.4	[7]
LBV	CVCC	NH_3/C_2H_6/air	9:1–1:9	300	1	0.8–1.4	[8]
SP	JSR	$NH_3/C_2H_6/O_2/Ar$	9:1–4:1–1:1	700–1180	1	0.5–2.0	[3]

IDT—ignition delay time: LBV—laminar burning velocity; ST—shock tube; RCM—rapid compression machine; CVCC—constant volume combustion chamber; HF—Heat flux method; SP—Species mole fraction profiles.

The effect of the ethane addition on the oxidation of ammonia/natural gas blends was studied in [1]. The results for ignition delay time showed that the reactivity of ammonia/ethane blends is significantly higher than that of ammonia/methane and ammonia/natural gas blends. Furthermore, it was shown that for $NH_3/CH_4/C_2H_6$ blends, the heat release and temperature increase at the early stage of the autoignition are determined by ethane consumption. In [2], it was revealed that the presence of ethane significantly affects the first half of the ignition process (0–0.5 IDTs). The reason for this phenomenon is the formation of CH_3 radicals from the ethane. Ignition delay times for ammonia/ethane

blends were measured in [4] with particular attention paid to analyzing the effect of C/N reactions on the oxidation process.

The authors found that the reaction $C_2H_6 + NH_2 = C_2H_5 + NH_3$ accelerates the oxidation of C_2H_6, thereby increasing the system's reactivity. Conversely, the reaction $CH_2CHO + NH_2 = CH_2CO + NH_3$ retards the oxidation of the fuel blend. At high temperatures, the reactions $C_2H_3 + NH_2 = C_2H_2 + NH_3$ and $HCO + NH_2 = CO + NH_3$ primarily contribute to the reduction in reactivity. Using a shock tube, Li et al. measured ignition delay times and the time-dependent concentrations of CO, NH_3, and NO using laser absorption spectroscopy [5]. The study demonstrated that, at high temperatures, the transition from lean to rich blends results in the increase in ignition delay time. For NH_3/C_2H_6 blends, it was revealed that CO concentration reaches its peak earlier compared to NO, indicating that reactions involving nitrogen-containing species take place at higher temperatures.

Ignition delay times were measured in a rapid compression machine by Li et al. [3]. Additionally, the study presents experimental data on the mole fraction profiles for ammonia/ethane blends oxidation in a jet-stirred reactor. The dependence of NH_3, C_2H_6, H_2, C_2H_4, CH_4, CO, NO, NO_2, HCN, CH_2O, HNCO, and CH_3CHO concentrations on the reactor temperature for $NH_3/C_2H_6/O_2/Ar$ fuel blends of various compositions was measured using mass spectrometry. Analysis of sensitivity coefficients revealed that the presence of ethane decreases the self-ignition temperature due to the reaction of NH_2 with C_2H_6. When the ethane fraction in the fuel blend is 50%, the primary contributing reactions are those of C_2H_6 with HO_2 and the decomposition of H_2O_2 forming OH. For the oxidation in a jet-stirred reactor, the process is predominantly influenced by reactions $NH_2 + C_2H_6$, $NH_2 + C_2H_4/CH_3$, $H + O_2$, and reactions involving HCO.

Wang et el. measured laminar burning velocity of NH_3/C_2H_6 blends [6]. The authors proposed two mechanisms: the reduced one, based on the model of light hydrocarbons combustion [9] in which the sub-mechanism of nitrogen-containing species was updated using the work of Okafor et al. [10]; and the second, more detailed mechanism, based on the model of butane isomers combustion [11]. The sub-mechanism of N-containing species for the latter was adopted from the works of Glarborg et al. [12,13] and Zhang et al. [14]. Numerical simulation and its subsequent analysis showed that the decrease in burning velocity with ammonia addition occurs primarily due to its reactions with H and OH radicals, while cross (C/N) reactions have a much smaller effect. Chen et al. also measured laminar flame speed of NH_3/C_2H_6 blends [7]. The authors also studied the effect of ozone addition on burning velocity. At the early stages of ozone decomposition, O radicals are formed and subsequently participate in chain branching reactions.

Zhang et al. measured the laminar flame speed of NH_3/C_2H_6 blends using a constant-volume combustion chamber and performed numerical simulations [8]. The comparison of experimental and numerical data indicates the importance of accurate consideration of C/N reactions in the mechanism.

In a recent paper [15], 18 detailed reaction mechanisms for $NH_3 + H_2$ mixtures and 13 mechanisms for $NH_3 + H_2 + CO$ mixtures were analyzed. For NH_3/H_2 mixtures, the best agreement with the ignition delays measurements, speciation in JSR, and laminar burning velocity was shown by the following mechanisms: POLIMI-2020 [16,17], Han-2020 [18], and KAUST-2021 [14]. For NH_3/syngas mixtures, the experimental data was better described by the mechanisms of Shrestha-2021 [19], Mei-2021 [20], and Mei-2020 [21]. The results of this work indicate that even for the relatively simple systems such as $NH_3 + H_2$ and $NH_3 + H_2 + CO$, there is no single universal mechanism capable of describing the entire set of experimental data with sufficient accuracy.

In the work of Yin et al. [22], the oxidation of $NH_3 + C_3H_8$ mixtures in JSR was studied experimentally. The authors also proposed the detailed chemical kinetic mechanism, which

satisfactorily described NH_3 + C_3H_8 oxidation in JSR and enabled them to reveal the main consumption pathways of fuel components in this system. The analysis showed that the propane conversion products—IC_3H_7, CH_3, and HCO—promote low-temperature oxidation of NH_3 by influencing the radical pool—OH and HO_2. Under fuel-rich conditions, the interaction of nitrogen- and carbon-containing intermediate compounds results in the formation of methylamine (CH_3NH_2), which is a source of HCN according to the following scheme: $CH_3NH_2 \rightarrow CH_2NH_2 \rightarrow CH_2NH \rightarrow H_2CN/HCNH \rightarrow HCN$.

In the work of Shrestha et al. [23], the oxidation of NH_3 + CH_3OH and NH_3 + C_2H_5OH mixtures was studied. The authors measured the laminar burning velocity and the ignition delays over a wide range of pressures, temperatures, and the fractions of CH_3OH or C_2H_5OH in the mixture with NH_3. The results showed that C_2H_5OH is a more effective combustion promoter, increasing the reactivity of NH_3 and reducing NOx emissions more effectively than CH_3OH. The authors also proposed a new mechanism, which demonstrated good predictive capability for NH_3 mixtures with other fuels.

The above literature review indicates that there are currently no experimental data on the flame structure of NH_3/C_2H_6 blends and on the ignition delay times of $NH_3/C_2H_6/O_2/Ar$ blends in the temperature and pressure range of 1300–1600K and 7–8 atm, respectively.

Therefore, the aim of this work is twofold. First, to extend the experimental database on the combustion and oxidation of $NH_3/C_2H_6/O_2/Ar$ blends. This includes obtaining data on (1) the chemical structure of premixed flames at the pressure of 1–5 atm; (2) ignition delay times in a shock tube; and (3) the species composition in a jet-stirred reactor over a range of temperatures. Second, to compare the results of numerical simulation performed using the most recent detailed chemical–kinetic models of NH_3/C_2H_6 blends' oxidation. The most adequate model will be used to analyze the effects of pressure and the initial composition on the formation of intermediate products and the pathways of ammonia–ethane interaction. The selected model was also modified to improve its predictive capability.

2. Experiment

2.1. Flame Structure

In this work, the structure of premixed ammonia/ethane/oxygen/argon flames (ϕ = 0.8, 1.0, 1.2) was measured at 1, 3, and 5 atm. The NH_3/C_2H_6 ratio was maintained at 1/1 in all experiments. The experiments were performed using a molecular beam mass spectrometric setup with soft electron impact ionization. A detailed description of the setup, flame stabilization system, and data processing procedure are presented in our previous works [24–27].

The flames were stabilized on the flat burner, and their temperature was 368K in all experiments. This burner was specially designed for ammonia flames and ensures stabilization at both atmospheric and elevated pressures. Its parameters are given in [28]. In the experiments at elevated pressures, the burner was placed in a special high-pressure chamber. Its construction is described in detail in the work presented in [28].

To ensure a more accurate analysis of pressure and temperature effect on intermediates concentration, specific attention was paid to the selection of flame stabilization conditions. Table 2 shows the composition of unburnt gas blends and flame stabilization conditions. In total, the structure of nine flames was measured in this study.

Table 2. The composition of unburnt gas blends and stabilization conditions for $NH_3/C_2H_6/O_2$ /Ar flames.

φ	*p*, atm	Reactants Mole Fraction				Mass Flow Rate [g/(cm^2×s)]
		NH_3	C_2H_6	O_2	Ar	
1.0	1/3/5	0.04	0.04	0.17	0.75	0.026
0.8	1/3/5	0.03	0.03	0.18	0.75	0.026
1.2	1/3/5	0.04	0.04	0.16	0.75	0.021

Since the flame sampling technique was applied in this work, it is essential to use a probe with geometric parameters suitable for both atmospheric-pressure and high-pressure experiments. The probe parameters are provided in [28]. The descriptions of molecular beam formation and the ionizing system are given in the previous works [24–27]. Our setup enables us to set the value of ionizing electrons energy (E) individually for each species. It is crucial to select a value of E that is sufficiently higher than ionization potential while simultaneously minimizing the overlap with other peaks in the mass spectrum. The mass spectrometer used in this work is equipped with a specialized ion source with an ionizing electron energy spread of ±0.25 eV (in the range of 12.3–18 eV). It enables the effective separation of the species with identical molecular masses if their ionization potentials differ by more than 0.5 eV.

In this work, the concentration profiles were measured for the following species: C_2H_6, NH_3, O_2, CO_2, N_2, H_2O, NO, CO, HCN, C_2H_2, C_2H_4, C_3H_4, C_3H_6, CH_2CO, CH_3CHO, HO_2, H_2O_2, CH_3, and NH_2. The mass spectrometer used does not enable us to separate allene (aC_3H_4) and propyne (pC_3H_4) and propene (C_3H_6) and ketene (CH_2CO). Therefore, for these species, total concentration profiles are provided further. Table 3 shows the ionizing electrons energy values, the calibration method for each species, and the corresponding measurement accuracy.

The procedure of intensity recalculation to mole fraction, along with the calibration procedures, are described in [28]. Table 3 provides the calibration method for each species.

The overall uncertainty for each species includes the following contributions: (1) statistical uncertainty in the intensity measurement of a particular mass peak; (2) the uncertainty in setting the gas flow rates at the burner inlet; (3) uncertainty associated with subtracting fragment contributions or overlapping mass spectra from compounds with identical molecular masses; (4) the uncertainty in determining the calibration coefficient Si in direct calibrations; (5) the uncertainty in the RICS calibration method; and (6) uncertainty in estimating the ionization cross sections of the compounds.

Temperature profiles were measured with thin S-type thermocouples (Pt/Pt + 10% Rh), manufactured from a 50 µm diameter wire. A detailed description of the thermocouple design and temperature measurement procedure is provided in our previous work [29].

Since the flame sampling technique was used for flame structure measurement, it is necessary to account for gas-dynamic perturbations introduced by the probe. This was performed by shifting the concentration profiles by a fixed distance towards the burner surface. The procedure of the shift-value estimation is provided in the work presented in [26]. In particular, in this work it was approximately 0.3 mm.

Table 3. Measured species. IE: ionization potential (reference data); E: energy of ionizing electrons.

m/*z*	Formula	IE (eV)	E (eV)	Calibration Type	Accuracy
15	CH_3	9.84	12.3	RICS(CH_4)	±50%
16	NH_2	10.78	12.3	RICS(NH_3)	±50%
16	CH_4	12.61	13.2	Direct	±50%
17	NH_3	10.07	12.5	Direct	±20%
18	H_2O	12.62	15.4	O-balance	±20%
26	C_2H_2	11.41	12.3	Direct	±50%
27	HCN	13.71	18.0	RICS(C_2H_4)	±50%
28	C_2H_4	10.53	12.3	Direct	±50%
28	CO	14.01	15.4	Direct	±20%
28	N_2	15.58	16.65	Direct	±20%
30	NO	9.26	10.8	Direct	±20%
30	C_2H_6	11.55	12.3	Direct	±20%
32	O_2	12.07	14.35	Direct	±20%
33	HO_2	11.35	16.65	RICS(O_2)	±50%
34	H_2O_2	10.58	14.35	Direct	±50%
40	aC_3H_4 + pC_3H_4	10.22/10.48	13.2	RICS(CO_2)	±50%
42	C_3H_6 + CH_2CO	9.74/9.62	12.3	RICS(CO_2)	±50%
44	CH_3CHO	10.22	12.3	RICS(CO_2)	±50%
44	CO_2	13.78	15.4	Direct	±20%

RICS—relative ionization cross-section method.

2.2. Oxidation in a Jet-Stirred Reactor

The oxidation of $NH_3/C_2H_6/O_2/Ar$ blends (φ = 0.5, 1.0 and 2.0) was studied in an isothermal jet-stirred reactor. In all experiments, the initial mole fraction of ammonia was 0.005, and the NH_3/C_2H_6 ratio was 1:1. The experiments were performed at atmospheric pressure over the temperature range of 800–1300 K. The residence time of the gas mixture inside the reactor was 1 s. The reactor volume is approximately 76 cm^3. The detailed description of the experimental setup with a jet-stirred reactor is presented in our previous work [30].

The gas composition was analyzed using a Hiden HPR-60 mass spectrometric complex. Unlike the setup described in the previous section, the energy of ionizing electrons was 70 eV. In this work, the concentrations of the following species were measured: NH_3, C_2H_6, O_2, CO, N_2, H_2O, CO_2, HCN, NO, CH_4, and H_2. Signal intensities were converted to mole fractions using the procedure identical to that described in the previous section.

2.3. Ignition Delay Time Measurement

Experiments on ignition delay time measurements of stoichiometric ammonia–ethane–oxygen blends were performed using a shock tube of standard diaphragm design. The geometric parameters, setup construction, blends preparation, and the description of the data acquisition system are detailed in [31].

The blends composition and experimental parameters are provided in Table 4. Due to the technical limitations of the shock tube, the pressure behind the reflected shock wave exhibited both variations during the experiment and a systematic shift towards lower values. For numerical simulations, the median pressure value in each series was used (shown in Table 4).

Table 4. Blends used in the shock tube experiment and calculated parameters of the gas behind the reflected shock waves.

Blend	Mole Fractions, %				*p*, atm	Pmed, atm	T, K
	NH_3	C_2H_6	O_2	Ar			
30%_C_2H_6	6.53	0.6	7	85.87	7.7–8.6	8.0	1270–1460
10%_C_2H_6	8.4	0.2	7	84.40	6.7–8.0	7.7	1370–1590

The ignition delay time was measured using the widely applied method of detecting the emission signal from the excited OH* radical, which is characteristic for both hydrocarbons and ammonia combustion. Simultaneously with the increase in OH* emission intensity, the pressure increase in the studied section of the shock tube was recorded. The ignition moment was defined as the intersection of the tangent at the point of maximum slope of the OH* radiation signal with its base level. The uncertainty of a single ignition delay time measurement, determined by the signal-to-noise ratio, was approximately 15 μs.

3. Numerical Modeling

Numerical modeling in this work was performed using CHEMKIN and Cantera.

The flame structure was simulated using the PREMIX code. The GRAD and CURV parameters were 0.1 and 0.2, respectively. Mixture-averaged transport and thermo-diffusion options were taken into account. Experimentally measured temperature profiles were used as input data for modeling, enabling us to consider the probe presence effect.

Mole fraction profiles of species formed during oxidation in an isothermal jet-stirred reactor were simulated using the PSR (perfectly stirred reactor) module. To obtain a steady-state solution, a transient solver with the end time of 20 s was used.

Ignition delay times were simulated with the constant volume reactor model using Cantera code. Ignition delay time was determined similarly to the method described in the previous section: the moment of ignition was defined by a sharp increase in OH concentration.

Numerical modeling was performed using 11 published detailed chemical kinetic mechanisms listed in Table 5. It should be noted that ethane and ammonia are present in many reaction mechanisms; therefore, it is not possible to test them all in this work.

Table 5. Mechanisms used for numerical modeling.

Name of the Detailed Reaction Mechanism	Number of Species	Number of Reactions	Year	Ref.
Model 1	187	1446	2023	[3]
Model 2	92	472	2023	[7]
Model 3	193	1468	2024	[4]
Model 4	192	1504	2024	[5]
Model 5	2	340	2025	[8]
Model 6	2854	11,797	2024	[1]
Model 7	188	1604	2022	[6]
Model 8	125	1099	2020	[19]
Model 9	356	2309	2023	[22]
Model 10	159	2459	2020	[16,17]
Model 11	285	2346	2025	[23]
pr. work	285	2346	2025	present work

As discussed in the next Section, model 11 [23] provides the best agreement with the experimental data for the $NH_3/C_2H_6/O_2/Ar$ mixtures' oxidation in JSR. However, model 11 shows larger discrepancies for IDT compared to model 6 [1] and model 8 [19]. For the flame structure, model 11 provides good agreement for reactants and main combustion products and acceptable qualitative agreement with the other species. Therefore, the sensitivity analysis for IDT was performed. Figure 1 shows a short diagram of the sensitivity coefficients for the reactions with the largest contribution and that received the most attention in this paper. The analysis was performed at 8 atm and 1400 K, since these values are representative for shock tube experiments, presented in the current paper.

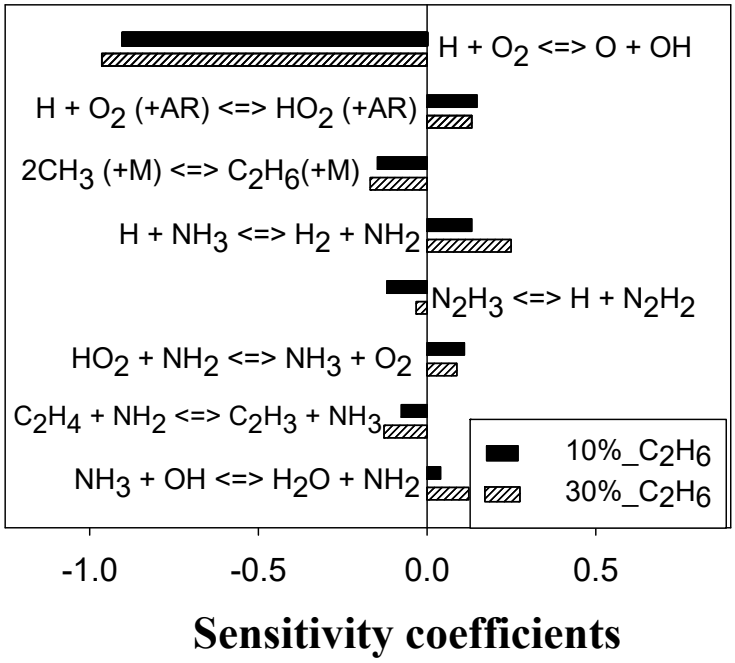


Figure 1. Short diagram of the sensitivity coefficients for IDT of $NH_3/C_2H_6/O_2/Ar$ mixtures (ethane content was 10% and 30%, p = 8 atm, T = 1400 K).

As shown in Figure 1, the highest sensitivity is observed for the reaction H + O_2 = O + OH. Other important reactions include H + O_2(+AR) <=> HO_2(+AR) and $2CH_3$(+M) <=> C_2H_6(+M). The rate constants of these three reactions were not adjusted in this work, since they are considered to be well-established. The rate constants for the reactions H + NH_3 <=> NH_2 + H_2 and NH_3 + OH <=> H_2O + NH_2 were adopted from model 6, since they are similar in models 11 [23] and 8 [19]. The rate constant for the NH_2 + HO_2 <=> NH_3 + O_2 reaction was adopted from model 8 [20] since model 6 includes the reverse reaction. The rate constant for the reaction C_2H_4 + NH_2 <=> C_2H_3 + NH_3 was taken from model 6, since it is absent in model 8. The rate constant for the reaction N_2H_3 <=> H + N_2H_2 was not updated, since it is similar in all three models.

Therefore, the model "pr.work" (Table 5) is the modification of model 11 with four updated rate constants, mentioned above.

4. Results and Discussion

4.1. Flame Structure

First, the experimentally measured temperature profiles are shown on Figure S1 (from Supplementary Material). Flame stabilization conditions were selected to ensure the closest possible temperature values in the post-flame zone. This approach enables us to neglect the temperature effect in the subsequent data analysis. The values of temperature in the post-flame zone are shown on the corresponding graphs.

Further the results on the species concentration profiles are discussed. Since quite a few systems were investigated in this work, only the most important results are present in the main text. The others are included in Supplementary Material.

Figures 2 and S2–S10. show the concentration profiles of the reactants (NH_3, C_2H_6, O_2) and main combustion products (CO_2, N_2, H_2O) in the stoichiometric $NH_3/C_2H_6/O_2/Ar$ flame at 5 atm. Here, further simulation results of the most representative mechanisms are presented in the main text. The results of numerical simulations using 12 mechanisms are presented in Supplementary Material. For these species, all tested models provide agreement within the experimental uncertainty and are consistent with each other. This trend is observed for all studied flames. The calculated and measured concentrations of combustion products become close to thermodynamic equilibrium values at the height above the burner (HAB) greater than 0.4 mm.

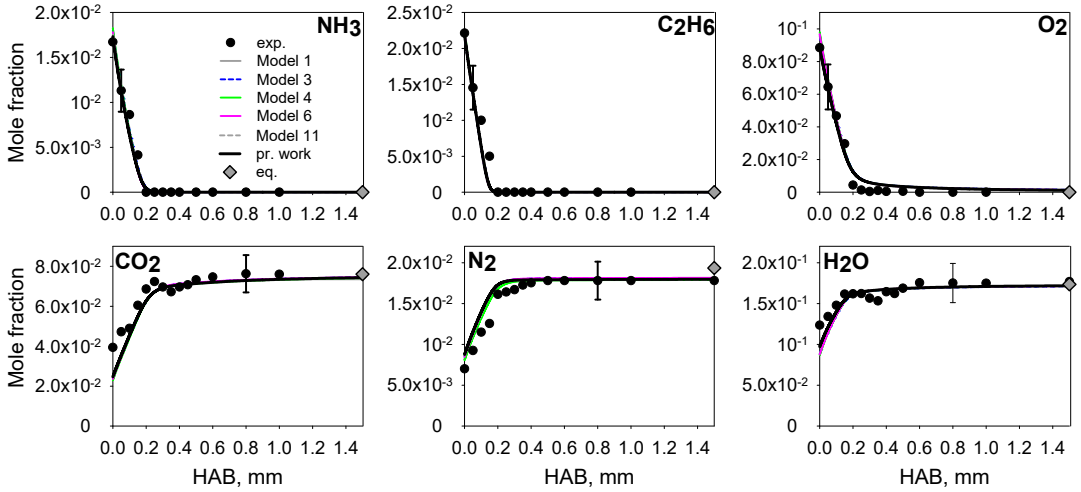


Figure 2. Mole fraction profiles of reactants and main combustion products in stoichiometric $NH_3/C_2H_6/O_2/Ar$ flame (φ = 1.0, p = 5 atm). Symbols: experimental data; lines: modeling results.

Figure 3 shows the mole fraction profiles of C-containing species, CO and HCN, measured in rich flames at 1–5 atm. Results for lean and stoichiometric conditions are provided in Figures S11–S13. For CO, the quantitative agreement between experimental and numerical data is significantly better than for HCN. This may be due to inaccuracy in determining the sensitivity coefficient for HCN. Moreover, for CO models demonstrate quite close results, while for HCN significant differences are observed. The predicted HCN peak concentrations differ by one order. However, all the models provide sufficient qualitative agreement, correctly describing the shape of the HCN mole fraction profile and the position of its peak concentration.

The observed discrepancies among the models for HCN may be attributed, in particular, to the different set (or absence) of C/N reactions. In the post-flame zone, the measured CO concentration is close to the thermodynamic equilibrium value; this trend is shown by most of the models. The measured HCN concentration in the post-flame zone (at 2 mm from the burner surface) is several orders higher than its thermodynamic equilibrium concentration.

Figure 4 shows the mole fraction profiles of C_2-hydrocarbons (C_2H_2 and C_2H_4) registered in rich flames. The corresponding results for lean and stoichiometric flames are shown in Figures S14 and S15. In general, all six models correctly reproduce the profiles shape and the position of the peak concentration. However, in rich conditions, models 5, 8, 9, and 10 overestimate C_2H_2 concentration in the post-flame zone, and this discrepancy with other models becomes pronounced at 5 atm. Moreover, there are quantitative differences

between the numerical peak concentrations, and the largest discrepancy is approximately 2 times.

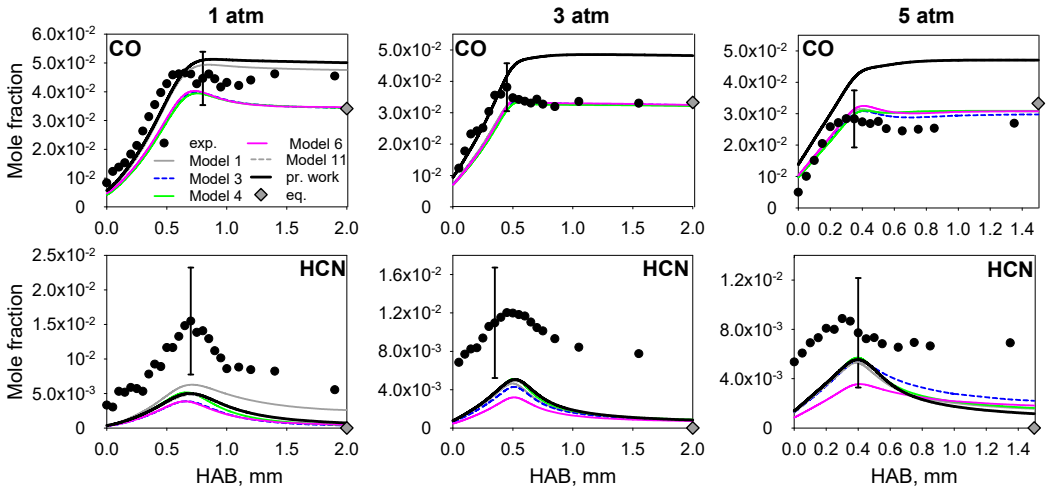


Figure 3. Mole fraction profiles of CO and HCN in rich $NH_3/C_2H_6/O_2/Ar$ flames (φ = 1.2, p = 1–5 atm). Symbols: experimental data; lines: modeling results.

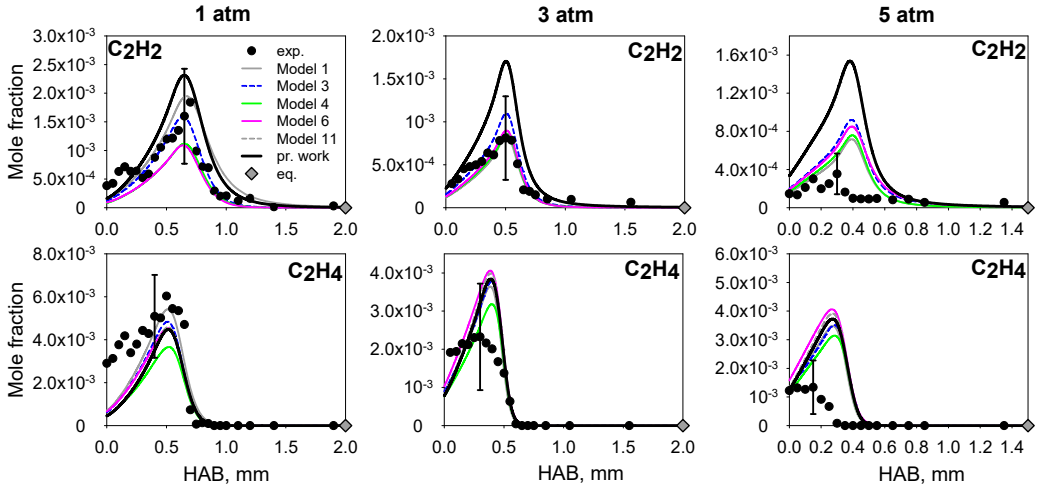


Figure 4. Mole fraction profiles of C_2H_2 and C_2H_4 in rich $NH_3/C_2H_6/O_2/Ar$ flames (φ = 1.2, p = 1–5 atm). Symbols: experimental data; lines: modeling results.

As demonstrated in previous works [28,32], among NOx, only NO is present in the post-flame zone in a significant concentration. Therefore, this work focuses specifically on NO. Figure 5 shows experimentally measured and simulated NO mole fraction profiles in lean flames, since NO concentration is higher under lean conditions compared to stoichiometric and rich ones (Figure S18 and Figure S19, respectively). A number of studies have shown that during the combustion of rich NH_3/H_2 and NH_3/CH_4 mixtures, the concentration of NOx in the combustion products is significantly lower than in the case of lean and stoichiometric mixtures [32–37]. This indicates that the effect of equivalence ratio on NOx formation in NH_3/C_2H_6 flames is the same as in NH_3/H_2 and NH_3/CH_4 flames.

As shown, the models predict different NO concentrations both in the post-flame zone and the peak (φ = 1.2, Figure S19). Moreover, the agreement between experimental and numerical data deteriorates with the pressure increase. At atmospheric pressure, almost all models provide agreement within experimental uncertainty. The pressure increase to 3 and 5 atm results in more significant discrepancies.

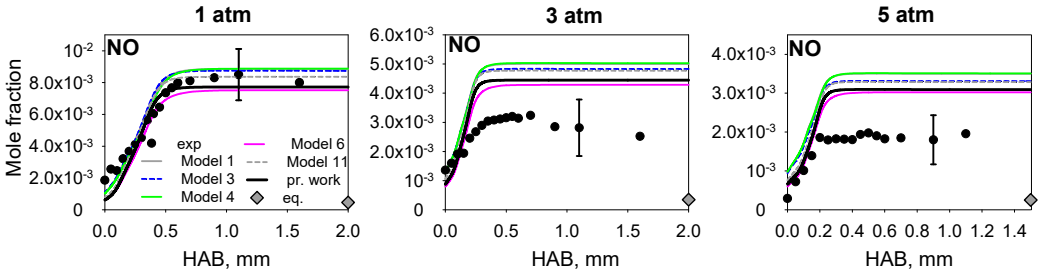


Figure 5. Mole fraction profiles of NO in lean $NH_3/C_2H_6/O_2/Ar$ flames (φ = 0.8, p = 1–5 atm). Symbols: experimental data; lines: modeling results.

Figure 6 shows the mole fraction profiles of aC_3H_4 + pC_3H_4, C_3H_6 + CH_2CO and CH_3CHO in rich conditions. In lean flames, allene and propyne were not registered (Figure S20), while in stoichiometric conditions, only propene and ketene were measured (Figure S21). Since the mass spectrometer used in the work is not able to resolve the signals of allene/propyne and propene/ketene, their total profiles are presented. It should first be noted that models 1, 3, 4, and 5 do not include reactions involving C_3-hydrocarbons. Consequently, for the total mole fraction profile of C_3H_6 and CH_2CO, for models 1, 3, 4, and 5, only the profile of CH_2CO is shown. Model 8 includes a limited number of reactions with allene and propyne, which, in turn, results in the incorrect shape of their total concentration profile.

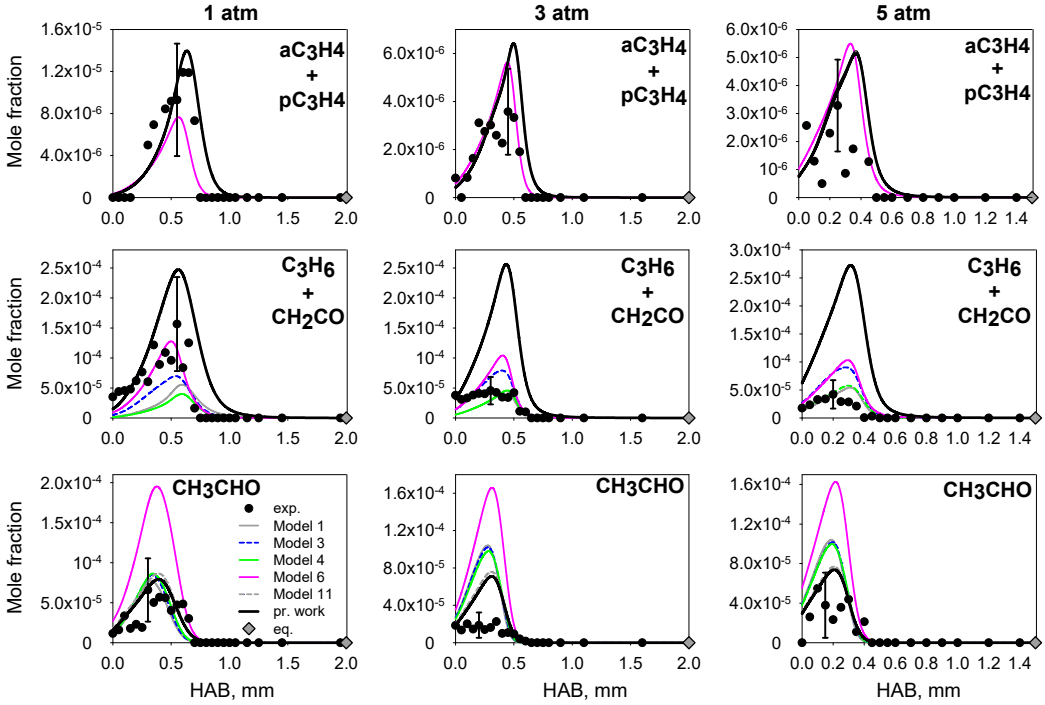


Figure 6. Mole fraction profiles of CH_3CHO, C_3H_6 + CH_2CO and aC_3H_4 + pC_3H_4 in rich $NH_3/C_2H_6/O_2/Ar$ flames (φ = 1.2, p = 1–5 atm). Symbols: experimental data; lines: modeling results. (For C_3H_6 + CH_2CO numerical results obtained with models 2 and 5 are divided by 10. For CH_3CHO numerical results obtained with models 1, 3, and 4, they are divided by 10. Experimental data for CH_3CHO at 5 atm is multiplied by 10.).

Overall, there is qualitative agreement between experimental and numerical data. However, measurement accuracy for these species is very low due to their low concentration in the flame. Therefore, it is almost impossible to draw conclusions regarding quantitative agreement with the modeling results.

Models 6 and 9 predict a significantly higher peak concentration of C_3H_4 compared to model 2 (the difference is 3–4 times). Models 7, 11, and the model from the present work predict even higher total peak concentration of these species, approximately 1.5 times higher than that predicted by model 6.

Although the concentration of C_3H_6 and CH_2CO is higher compared to C_3H_4, a quantitative assessment of model agreement still remains difficult. First of all, the measurement accuracy for these species is quite low. Secondly, C_3H_6 and its reactions are present only in the part of models tested. However, qualitative agreement is acceptable since the tested models correctly reproduce the concentration profiles' shape and peak position. For CH_3CHO, there is also good qualitative agreement between the experimental and numerical data, considering the large measurement uncertainty. Models 2 and 7 predict the lowest peak concentration compared to other models. According to model 5, the CH_3CHO peak is located farther from the burner surface compared to other models.

The mole fraction profiles for other species registered in the studied flames are presented in Supplementary Material. Methane profiles are shown in Figures S23 and S24. In lean flames, methane was not registered due to its low concentration. According to Figures S23 and S24, the measured and simulated peak concentration of methane changes only slightly when the pressure increases from 1 to 3 atm. However, the further pressure increase to 5 atm decreases the experimental value by almost an order and the numerical one only slightly. In general, there is satisfactory qualitative agreement between experimental and numerical data. One reason for quantitative discrepancies may be attributed to the contribution of fragment ions from ammonia and other heavier species.

Figures S25–S27 show the mole fraction profiles of HO_2 and H_2O_2. The accurate prediction of these species is important, particularly for ensuring good predictive capability at low temperatures. In general, the obtained results show good qualitative agreement between the experimental and numerical data. The observed discrepancies of the absolute values can be attributed to the low measurement accuracy, which appears due to low concentration of HO_2 and H_2O_2.

The concentration profiles of key radicals in ammonia/ethane flames—CH_3 and NH_2—are given in Figures S28–S30. The ability to register radicals is important to substantiate the probe sampling method. While qualitative agreement exists between the experimental and numerical data, the quantitative agreement for NH_2 is significantly better than for CH_3. For the latter, the discrepancy in peak concentration is 30–70 times. This may be associated with a larger uncertainty in the CH_3 sensitivity coefficient and larger contribution of fragment ions.

4.2. Oxidation in a Jet-Stirred Reactor

It was previously established that adding 30% of hydrogen to ammonia reduces the onset temperature of the mixture oxidation by 250 K [30]. Methane addition acts similarly to hydrogen, as it also leads to a decrease in the onset temperature of the mixture oxidation [38–42]. As can be seen in Figure 7, the onset temperature of $NH_3/C_2H_6/O_2/Ar$ mixture oxidation is about 900 K, which is approximately 300 K lower than that for pure ammonia [30]. This indicates that the effect of C_2H_6 addition is similar to that of adding hydrogen or methane.

Figure 7 shows the concentration of reactants and oxidation products vs. temperature in the lean $NH_3/C_2H_6/O_2/Ar$ blend. It should be noted that in Figure 7, simulation results obtained only with models 1, 3, 4, 6, and 11 and that from the present work are shown. The complete set of modeling for all models is provided in Supplementary Material (Figure S32). As seen, models 2, 5, 7, 8, 9, and 10 are inconsistent with the experimental results; therefore, they will not be discussed in this section.

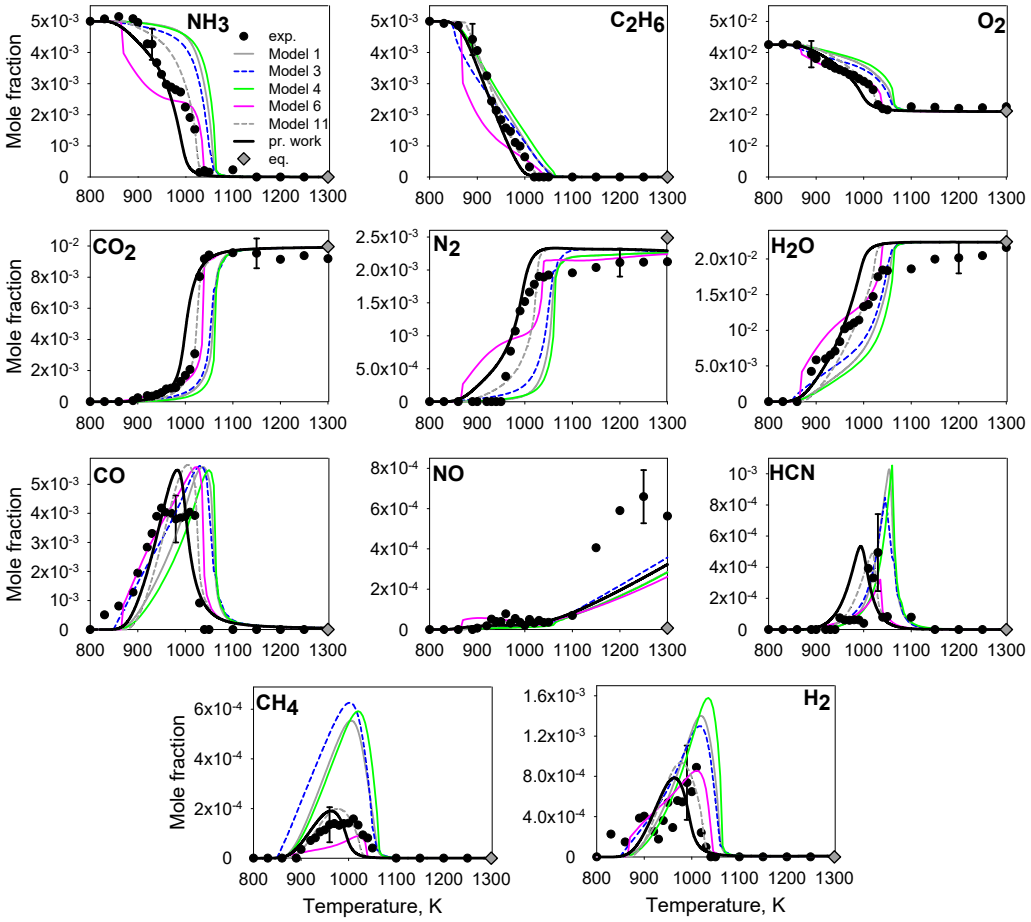


Figure 7. Species concentration vs. reactor temperature in lean $NH_3/C_2H_6/O_2/Ar$ blend (φ = 0.5, τ = 1 s, p = 1 atm, NH_3 fraction = 0.005, NH_3/C_2H_6 = 1/1). Symbols: experimental data; lines: modeling results. (For H_2, experimental data is multiplied by 10.)

Model 6 predicts faster oxidation of the studied blend. Conversely, models 1, 3, and 4 overpredict the onset temperature of intensive oxidation. For NH_3, C_2H_6, O_2, CO_2, N_2, and H_2O, the best agreement is provided by model 11 and the model from the present work. Regarding CO and NO, models give relatively close results; however, quantitative agreement is better for CO than for NO, since NO's experimental concentration is higher compared to modeling values. For HCN and CH_4, the best agreement is provided by model 11 and the model from the present work. Figure 7 shows H_2 concentration that was multiplied by 10; thus, it is possible to assess only qualitative agreement, which appears acceptable.

Under stoichiometric conditions (Figure S31), models 2, 5, 7, 8, 9, and 10 are inconsistent with experimental data. However, for model 6, the discrepancies observed at low temperatures are less pronounced than for the lean blend. The overall tendency regarding agreement between experimental and numerical data is similar.

For the rich blend (Figure S33), the discrepancies shown by models 6 and 9 are even less significant. The behavior of NH_3, C_2H_6, O_2, CO_2, N_2, H_2O, and CO is adequately captured by all models. In the case of CH_4, all models overestimate its concentration. For HCN, model 6 provides the best agreement for its concentration at high temperatures. For H_2, only qualitative agreement is observed.

Figures S31–S33 show the species concentrations at thermodynamic equilibrium. For the rich blend, a larger difference exists between species concentration at 1300 K and the corresponding equilibrium values. This indicates that chemical processes proceed more slowly under rich conditions compared to stoichiometric and lean ones.

4.3. Ignition Delay Time

According to the available data, the addition of hydrogen to ammonia significantly reduces ignition delays under shock tube conditions [43–45] and in a rapid compression machine [46–48]. A similar effect is observed for methane addition. According to the published results, increasing the methane concentration reduces the induction time during autoignition behind a shock wave [49–51] and under adiabatic compression [52,53]. According to the results obtained in the present work, the effect of ethane addition on the ignition delays is similar to that for hydrogen or methane.

Figure 8 presents the ignition delay time vs. temperature of stoichiometric ammonia/ethane blends with 10% and 30% C_2H_6 content. As shown, models 2, 7, and 11 exhibit the largest discrepancies with the experimental data. For the mixture with 10% ethane, the best agreement is provided by models 3 and 8, whereas at 30% ethane, model 6 shows the best predictive capability. Therefore, as mentioned before, model 11 was updated. The resultant model shows acceptable agreement with the experimental data.

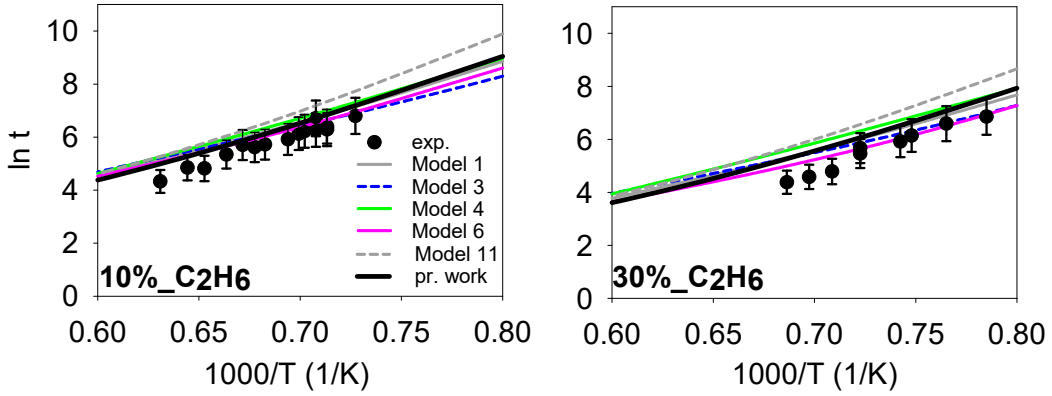


Figure 8. Ignition delay time vs. temperature for stoichiometric $NH_3/C_2H_6/O_2/Ar$ blends (C_2H_6 content 10% and 30%, p = 7.7 and 8 atm, respectively). Symbols: experimental data; lines: modeling results.

Additionally to comparison of the simulation results using the modified mechanism with experimental data on IDTs and speciation in flames and JSR, LBV simulations under conditions reported in [6–8] were also performed. The comparison showed that the largest discrepancies between experimental and numerical data are observed for blends with high ammonia content, which is also evident from IDTs (Figure 8). Furthermore, published data indicate that when the ammonia fraction in the mixture with ethane exceeds 50%, an increase in the scatter of experimental data is observed. Moreover, the discrepancy between the simulation results obtained with the modified mechanism and the published data increases with the equivalence ratio. Overall, the modified mechanism describes the published data on LBVs with satisfactory accuracy. The corresponding graphs are presented in Figures S42–S44 (Supplementary Material).

5. The Analysis of Pressure and Equivalence Ratio Effect on Intermediate Species Concentration in $NH_3/C_2H_6/O_2/Ar$ Flames

This section analyzes the effects of pressure and equivalence ratio on intermediate species concentration, which is crucial for optimizing fuel blend composition and combustion mode.

Figures S35 and S36 show the influence of pressure on NO, CO, and HCN concentrations in the post-flame zone (Figure S35) and on their peak mole fraction (Figure S36). Increasing pressure reduces both peak and post-flame zone concentrations of NO, and this trend is adequately captured by all models. In the study presented in [54], it was shown that

during the combustion of NH_3/H_2 blends, the pressure increase resulted into a decrease in NOx concentration. For ammonia/methane mixtures, it was also revealed that the increase in both pressure and equivalence ratio results in a decrease in NOx concentration [49,55,56]. This indicates that the effect of ethane addition to ammonia is similar to that of hydrogen or methane addition.

As expected, pressure also decreases CO concentrations, although this effect is less pronounced under rich conditions. All mechanisms adequately reproduce the pressure dependence of CO concentration. Pressure increase generally decreases HCN concentration, except the rich blends, where models predict either a slight decrease or a weak increase with pressure. It is known that in flames, the pressure increase accelerates the system's transition to a thermodynamically equilibrium state. The calculation of thermodynamically equilibrium concentrations of CO, HCN, and NO in $NH_3/C_2H_6/O_2/Ar$ mixtures at 1, 5, 20, and 100 atm and 1700 K (Table S1) show that as pressure increases, the CO and NO concentrations decrease. Although HCN concentration increases slightly, its absolute value is approximately 10 orders lower than CO and NO concentrations. Such data can be useful for analyzing the composition of engine combustion products.

Figure S37 presents C_2H_2, C_2H_4, C_3H_6 + CH_2CO, CH_3CHO, and CH_4 peak concentration vs. pressure. Their mole fractions in the post-flame zone are negligible. In the experiments, the peak concentration of C_2H_2 and C_2H_4 decrease with the pressure rise—a trend reproduced by all models. The total peak concentration of C_3H_6 + CH_2CO, measured in the experiment, also decreases with pressure; however, the models show different predictions. For CH_3CHO, the models also predict a different dependence on pressure. The measured peak concentration of CH_4 is significantly higher than simulated results. As noted previously, CH_4 was detected only in stoichiometric and rich flames. Numerical simulations show, as expected, the decrease in CH_4 peak concentration with pressure, except under rich conditions, where models predict different trends.

Figure S38 shows the total peak concentration of allene and propyne vs. pressure under rich conditions, where these species were detected. As mentioned above, C_3H_4-chemistry is included only in models 2, 6, 7–11, and in the present model. All these models correctly reproduce the experimentally observed decrease in C_3H_4 concentration with pressure. To explain the pressure effect, reaction rate analysis was performed. The reactions with the largest contribution to the species total formation/consumption rates are presented in Tables S2–S12. Overall, the presented data show that increasing pressure reduces the concentrations of intermediates to varying degrees. The most pronounced effect is observed for CO, HCN, C_2H_4, and CH_4, for which the ratio of consumption to formation reaction rates increases by a factor of 1.75, 1.13, 1.7, and 1.24, respectively, when pressure increases from 1 to 5 atm. For other intermediates, such as NO, C_2H_2, CH_3CHO, C_3H_6 + CH_2CO, and C_3H_4, the pressure increase leads to a weaker change in the ratio of their consumption-to-formation rates (ranging from 1.08 to 0.91). This explains the more modest change in their peak concentrations with increasing pressure.

Figures S39 and S40 show the effect of the equivalence ratio on the post-flame (Figure S39) and peak (Figure S40) concentrations of NO, CO, and HCN. All mechanisms adequately capture experimental trends: the decrease in NO concentration and sharp increase in CO and HCN concentration when transitioning from lean to rich conditions. For CO, there is also quantitative agreement between experimental and numerical results. Figure S41 presents the peak concentrations of C_2H_2, C_2H_4, C_3H_6 + CH_2CO, CH_3CHO, and CH_4 vs. the equivalence ratio. As expected, the concentrations of C_2H_2 and C_2H_4 are higher under rich conditions. Both experimental and numerical data show that CH_4 peak concentration increases with equivalence ratio. For these species, all models adequately capture the experimental tendency. Modeling data also predict the increase in the total peak

of C_3H_6 + CH_2CO with the equivalence ratio increasing. For CH_3CHO peak concentration, the tested models predict different dependence on the equivalence ratio.

6. Analysis of C_2H_6 and NH_3 Consumption Pathways

This section presents an analysis of the consumption pathways of the fuel mixture components—C_2H_6 and NH_3. This analysis was performed using the model from the present work, as it provides acceptable agreement with the entire set of experimental data. This model adequately reproduces the data obtained in a jet-stirred reactor, particularly the temperature range, corresponding to the intensive oxidation of the NH_3 + C_2H_6 blend. Moreover, this model includes cross-reactions involving C- and N-containing species. This is confirmed by the fact that HCN concentration predicted by this model is comparable with the experimental values. This is evident both from the flame structure data and from the oxidation data in JSR. This model also includes C_3-hydrocarbons and related reactions. Finally, it provides acceptable agreement with the ignition delay times for the NH_3 + C_2H_6 mixtures. The fact that this model provides quite good predictive accuracy indicates that it contains the most comprehensive set of reactions with the most correct rate consatnt parameters.

Figure 9 shows a scheme of the main consumption pathways of ethane and ammonia during oxidation in a jet-stirred reactor and in flame conditions. The analysis was performed for the stoichiometric mixture, since this equivalence ratio is intermediate among those studied.

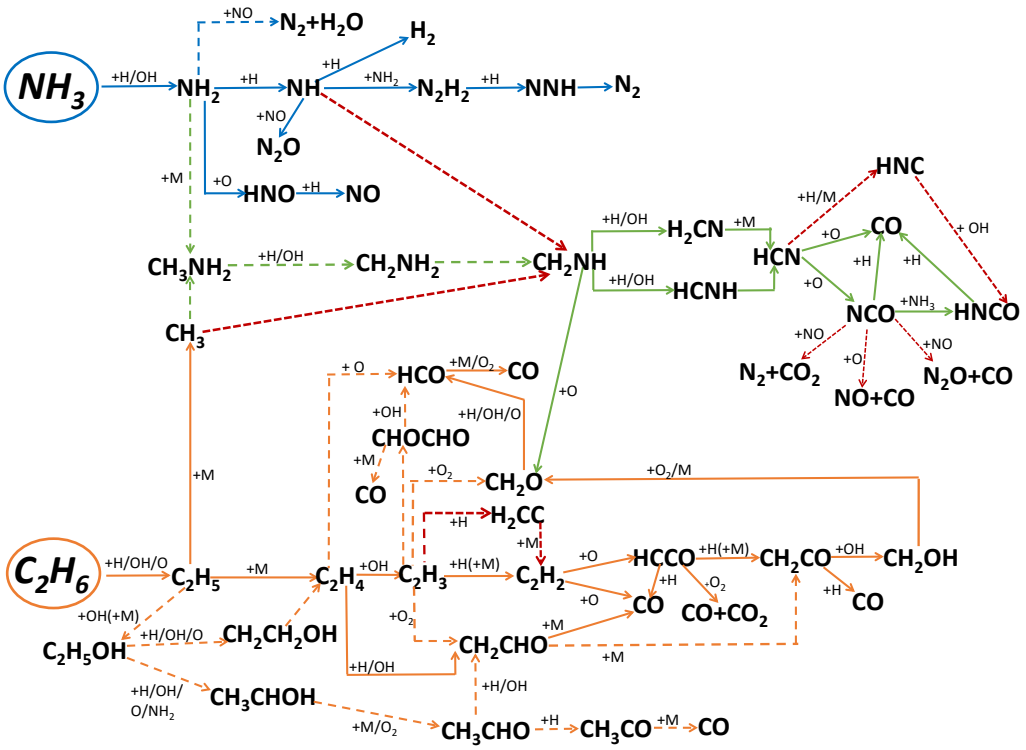


Figure 9. The main consumption pathways of ethane and ammonia during oxidation of stoichiometric $NH_3/C_2H_6/O_2/Ar$ blend in jet-stirred reactor (T = 1060 K) and in flame (1530 K). The scheme was obtained with the model from the present work. (Orange arrows indicate reactions involving C-containing species, blue arrows indicate reactions of N-containing species, and green arrows correspond to cross C/N pathways. Dashed arrows indicated the pathways which became less important at high temperatures. Red dashed arrows show the pathways which, on the contrary, appear at high temperature conditions.)

According to the obtained results, ethane oxidation occurs at slightly lower temperatures compared to ammonia. Therefore, the rate of ethane consumption reaches its maximum at a lower temperature. According to the model from the present work, the maximum rate of ethane consumption is observed at 1035 K and the maximum rate of ammonia consumption at 1090 K. Therefore, the analysis was performed at 1060 K, an intermediate value between the corresponding maxima for the two fuel components. It should be noted that only the pathways contributing more than 10% to the total consumption rate are shown in the scheme. In this Figure, orange arrows indicate reactions involving C-containing species, blue arrows indicate reactions of N-containing species, and green arrows correspond to cross C/N pathways. Dashed arrows denote pathways that become less significant at high temperatures. Red dashed arrows show the pathways which, conversely, appear at high temperature conditions. The decomposition of the C_2H_6 molecule occurs primarily through the formation of the C_2H_5 radical, which subsequently yields C_2H_4, CH_3, and C_2H_5OH. C_2H_4 then produces HCO, C_2H_3, and CH_2CHO. The C_2H_3 radical produces CH_2O, CHOCHO, C_2H_2, and CH_2CHO. The main products of CHOCHO decomposition are HCO and CO. The main product of HCO consumption is CO. CH_2O decomposition mainly yields HCO, which in turn produces CO. C_2H_2 mainly forms CO and HCCO. HCCO either produces CO or reacts with O_2 to form CO + CO_2. Another product of HCCO conversion is CH_2CO, which in turn yields CH_2OH and CO. CH_2OH decomposition results in CH_2O formation. CH_2CHO primarily yields CH_2CO. C_2H_5OH initially decomposes into two radicals: CH_2CH_2OH and CH_3CHOH. CH_2CH_2OH conversion results into C_2H_4 formation, whereas CH_3CHOH forms CH_3CHO. Further, CH_3CHO either produces CH_2CHO or CH_3CO, and the latter mainly decomposes to CO.

As can be seen, the consumption of hydrocarbon species occurs primarily in reactions with H, O, and OH. In contrast, reactions involving NH_2 contribute much less. As revealed in the works presented in [57,58], the interaction of hydrocarbons with NH_2 contributes significantly at low and intermediate temperatures, whereas at high temperatures their role is negligible.

The first step of NH_3 conversion is the formation of the NH_2 radical. Subsequently, NH_2 produces NH, HNO, and N_2 + H_2O. The main product of HNO consumption is NO. NH decomposition results into formation of N_2H_2, H_2, and N_2O. N_2H_2 produces NNH which in turn yields N_2. It should be noted that fuel-nitrogen in ammonia molecules is the main source of NOx. As can be seen from the scheme, NOx is mainly formed in reactions of ammonia-derived radicals (NH_2, NH) either with H (in the case of NO) or with NO (in the case of N_2O).

The first stage of C/N interaction is the reaction between CH_3 and NH_2, yielding CH_3NH_2. Further, CH_3NH_2 produces CH_2NH_2, which in turn yields CH_2NH. CH_2NH is the source of such species as HCNH and H_2CN. The main product of HCNH and H_2CN consumption is HCN. As is mentioned in the work in [22], under fuel-rich conditions the contribution of the CH_3 + NH_2 = CH_3NH_2 reaction increases. In the work in [22], the effect was around 20 times. Since CH_3NH_2 is the primary source of HCN, HCN concentration is consequently higher under rich conditions. HCN decomposition results into NCO formation. NCO yields CO and HNCO, and the latter decomposes to produce CO.

The temperature for the analysis at flame conditions was chosen similarly as described above. The maximum rate of ethane consumption takes place at 1455 K; for ammonia, this value is 1600 K. Consequently, an intermediate temperature of approximately 1530 K was selected for the analysis.

In flame conditions, most of the pathways are similar to those observed in an isothermal reactor. Therefore, for brevity, only the main differences will be discussed. The distinctive pathways are shown with dashed arrows. Regarding reactions involving C-

containing species, the pathway of C_2H_5OH formation becomes less significant along with the reactions of oxygenates (such as CH_3CHOH, CH_2CH_2OH, CH_3CO, CHOCHO, CH_2CHO, and CH_3CHO).

For N-containing species and their reactions, there are no significant differences; only the contribution of the $N_2 + H_2O$ formation's reaction from NH_2 is reduced. The most important difference in high-temperature from low-temperature conditions is that the initial step of C/N interaction proceeds via reaction of NH with CH_3 forming CH_2NH. The minor differences include pathways such as HCN->HNC->HNCO as well as pathways of $N_2 + CO_2$, NO + CO, and N_2O + CO formation from NCO.

Experiments in a shock tube were performed at pressures not significantly different from the flame conditions studied in this work, and the characteristic temperatures are comparable. Therefore, the scheme of C_2H_6 and NH_3 consumption pathways is expected to be very similar.

In general, ammonia and ethylene as individual fuels were studied in the substantial number of works. Therefore, it is assumed that chemical reactions of their consumption are well-known and largely similar across different mechanisms. It is important to note that while reactions involving C/N species have been studied in less detail, comparison with the published works reveals that these pathways are also generally quite similar in their mechanisms.

Nevertheless, it is important to note that the rate constants for individual reactions in these mechanisms may differ, which will lead to a certain discrepancy between experimental and numerical data. However, in our work, the rate constants were changed for only a few reactions, among which only one involves interaction of C- and N-containing species ($C_2H_4 + NH_2 <=> C_2H_3 + NH_3$). Therefore, this model modification will not lead to a significant change in the consumption pathways compared to the original model.

7. Conclusions

(1) A wide range of experimental data on the oxidation and combustion of ammonia/ethane mixtures was obtained. It includes data on $NH_3/C_2H_6/O_2/Ar$ blends' oxidation in a jet-stirred reactor *(φ = 0.5–2.0, NH_3/C_2H_6 = 1:1, p = 1 atm, τ = 1 s, T = 800–1300 K)*; data on the structure of $NH_3/C_2H_6/O_2/Ar$ flames *(φ = 0.8–1.2, NH_3/C_2H_6 = 1:1, p = 1–5 atm)*; and data on ignition delay time of $NH_3/C_2H_6/O_2/Ar$ blends *(φ = 1.0, NH_3/C_2H_6 = 11:1, 42:1, p = 6.7–8.6 atm, T = 1300–1600 K)*.

(2) Numerical modeling was performed for all studied systems using 11 published detailed chemical–kinetic mechanisms that contain the reactions of ammonia–ethane interaction.

(3) The comparison of experimental and numerical results indicated that currently none of the mechanisms are capable to describe all experiments from the present study. Therefore, the mechanism modification for the $NH_3 + C_2H_6$ mixtures was proposed, which resulted in improved agreement between experimental and simulated data.

(4) Based on the flame structure data, the effects of initial mixture composition (φ) and pressure on intermediate species concentration (both peak and in the post-flame zone) were analyzed. The increase in pressure and equivalence ratio decreases NO concentration. The concentration of C_2H_2, C_2H_4, CO, HCN, and CH_4 increases in rich conditions and decreases at higher pressures. For C_3H_4, only the pressure effect was analyzed, and pressure increase also results in a reduction in peak concentration. For C_3H_6 + CH_2CO and CH_3CHO, the models predict different trends of concentration change with the pressure and equivalence ratio.

(5) The effect of transition from relatively low-temperature oxidation to the flame combustion (and high-temperature oxidation) on the main pathways of ammonia and

ethane consumption was analyzed. Among reactions involving C-containing species, the pathways of oxygenate formation and consumption became less significant at high temperatures. The pathways involving N-containing species are almost similar at both low and high temperatures. At high temperatures, the first step of C-N interaction proceeds via reaction of NH with CH_3 forming CH_2NH. At low temperatures, it is the reaction of NH_2 and CH_3 which yields CH_3NH_2.

Supplementary Materials: The following supporting information can be downloaded at: https://www.mdpi.com/article/10.3390/app16020673/s1, Figures S1–S44, experimental data in Excel format, the updated mechanism. Table S1. The pressure effect on thermodynamically equilibrium concentrations of CO, HCN and NO; Table S2. Reactions with the largest contribution to the total CO consumption/formation rates; Table S3. Reactions with the largest contribution to the total HCN consumption/formation rates; Table S4. Reactions with the largest contribution to the total NO consumption/formation rates; Table S5. Reactions with the largest contribution to the total C_2H_2 consumption/formation rates; Table S6. Reactions with the largest contribution to the total C_2H_4 consumption/formation rates; Table S7. Reactions with the largest contribution to the total CH_4 consumption/formation rates; Table S8. Reactions with the largest contribution to the total CH_3CHO consumption/formation rates; Table S9. Reactions with the largest contribution to the total C_3H_6 consumption/formation rates; Table S10. Reactions with the largest contribution to the total CH_2CO consumption/formation rates; Table S11. Reactions with the largest contribution to the total aC_3H4 consumption/formation rates; Table S12. Reactions with the largest contribution to the total pC_3H_4 consumption/formation rates.

Author Contributions: Conceptualization, K.N.O.; investigation, K.N.O., V.V.M., A.V.D. and A.G.S.; formal analysis, K.N.O. and A.V.D.; writing—original draft preparation, K.N.O., A.V.D., S.A.T. and A.G.S.; supervision, A.G.S. All authors have read and agreed to the published version of the manuscript.

Funding: This work was funded by Russian Science Foundation, project No. 24-19-00165, https://rscf.ru/en/project/24-19-00165/ (accessed on 1 January 2026).

Data Availability Statement: The original data presented in the study are openly available in Supplementary Material.

Conflicts of Interest: The authors declare no conflicts of interest.

References

1. Jiang, Z.; Dong, S.; Gao, W.; Wang, B.; Ding, H.; Xie, J.; Zou, C.; Cheng, X. Probing the Effect of Fuel Components on the Auto-Ignition Behavior of Ammonia/Natural Gas Blends: A Case Study of Ethane Addition. *Combust. Flame* **2024**, *259*, 113186. [CrossRef]
2. Liu, B.; Zhou, M.; Zhang, Z.; Mi, X.; Belal, B.Y.; Li, G. Ignition Delay Times and Chemical Reaction Kinetic Analysis for the Ammonia–Natural Gas Blends. *Energy Fuels* **2024**, *38*, 1373–1382. [CrossRef]
3. Li, M.; He, X.; Zhu, D.; Fernandes, R.; Moshammer, K. Experimental and Kinetic Modeling Study of the Autoignition and Oxidation of Ammonia/Ethane Mixtures in a Rapid Compression Machine and a Jet-Stirred Reactor. *Combust. Flame* **2023**, *256*, 112931. [CrossRef]
4. Liu, J.; Dai, L.; Zou, C.; Peng, C.; Xia, W.; Lin, Q. A Shock Tube and Modeling Study of NH_3/C_2H_6 Combustion: Effects of C/N Cross-Reactions. *Combust. Flame* **2024**, *269*, 113652. [CrossRef]
5. Li, M.; Zhu, D.; Karas, H.; Agarwal, S.; Qu, Z.; Moshammer, K.; Fernandes, R.; Shu, B. NH_3/C_2H_6 and NH_3/C_2H_5OH Oxidation in a Shock Tube: Multi-Speciation Measurement, Uncertainty Analysis, and Kinetic Modeling. *Chem. Eng. J.* **2024**, *498*, 155041. [CrossRef]
6. Wang, D.; Wang, Z.; Zhang, T.; Zhai, Y.; Hou, R.; Tian, Z.Y.; Ji, C. A Comparative Study on the Laminar C_1–C_4 n-Alkane/NH_3 Premixed Flame. *Fuel* **2022**, *324*, 124732.
7. Chen, C.; Wang, Z.; Yu, Z.; Han, X.; He, Y.; Zhu, Y.; Konnov, A.A. Experimental and Kinetic Modeling Study of Laminar Burning Velocity Enhancement by Ozone Additive in NH_3+O_2+N_2 and NH_3+$CH_4/C_2H_6/C_3H_8$+air Flames. *Proc. Combust. Inst* **2023**, *39*, 4237–4246. [CrossRef]

8. Zhang, S.; Yue, W.; Zhang, B.; Xia, Y.; Wang, B.; Zhang, J. Study on the Mechanism for Laminar Burning Velocity Enhancement with Ethane Addition in Ammonia Premixed Flames. *Int. J. Hydrogen Energy* **2025**, *101*, 959–971. [CrossRef]
9. Williams, F.A. *Chemical-Kinetic Mechanisms for Combustion Applications*; University of California: San Diego, CA, USA, 2016.
10. Okafor, E.C.; Naito, Y.; Colson, S.; Ichikawa, A.; Kudo, T.; Hayakawa, A.; Kobayashi, H. Measurement and Modelling of the Laminar Burning Velocity of Methane-Ammonia-Air Flames at High Pressures Using a Reduced Reaction Mechanism. *Combust. Flame* **2019**, *204*, 162–175. [CrossRef]
11. Li, W.; Wang, G.; Li, Y.; Li, T.; Zhang, Y.; Cao, C.; Zou, J.; Law, C.K. Experimental and Kinetic Modeling Investigation on Pyrolysis and Combustion of N-Butane and i-Butane at Various Pressures. *Combust. Flame* **2018**, *191*, 126–141. [CrossRef]
12. Glarborg, P.; Andreasen, C.S.; Hashemi, H.; Qian, R.; Marshall, P. Oxidation of Methylamine. *Int. J. Chem. Kinet* **2020**, *52*, 893–906. [CrossRef]
13. Glarborg, P.; Miller, J.A.; Ruscic, B.; Klippenstein, S.J. Modeling Nitrogen Chemistry in Combustion. *Prog. Energy Combust. Sci.* **2018**, *67*, 31–68. [CrossRef]
14. Zhang, X.; Moosakutty, S.P.; Rajan, R.P.; Younes, M.; Sarathy, S.M. Combustion Chemistry of Ammonia/Hydrogen Mixtures: Jet-Stirred Reactor Measurements and Comprehensive Kinetic Modeling. *Combust. Flame* **2021**, *234*, 111653. [CrossRef]
15. Szanthoffer, A.G.; Zsély, I.G.; Kawka, L.; Papp, M.; Turányi, T. Testing of NH_3/H_2 and NH_3/syngas combustion mechanisms using a large amount of experimental data. *Appl. Energy Combust. Sci.* **2023**, *14*, 100127. [CrossRef]
16. The CRECK Modeling Group (Politecnico di Milano). NH_3 Mechanism (Version 2003, March 2020). 2020. Available online: https://www.creckmodeling.polimi.it/menu-kinetics/menu-kinetics-detailed-mechanisms/107-category-kinetic-mechanisms/400-mechanisms-1911-c1-c3-ht-nox/ (accessed on 1 January 2026).
17. Stagni, A.; Cavallotti, C.; Arunthanayothin, S.; Song, Y.; Herbinet, O.; Battin-Leclerc, F.; Faravelli, T. An experimental, theoretical, and kinetic-modeling study of the gas-phase oxidation of ammonia. *React. Chem. Eng.* **2020**, *5*, 696–711. [CrossRef]
18. Han, X.; Wang, Z.; He, Y.; Zhu, Y.; Cen, K. Experimental and kinetic modeling study of laminar burning velocities of NH_3/syngas/air premixed flames. *Combust. Flame* **2020**, *213*, 1–13. [CrossRef]
19. Shrestha, K.P.; Lhuillier, C.; Barbosa, A.A.; Brequigny, P.; Cotino, F.; Mounaïm-Rousselle, C. An experimental and modeling study of ammonia with enriched oxygen content and ammonia/hydrogen laminar flame speed at elevated pressure and temperature. *Proc. Combust. Inst.* **2021**, *38*, 2163–2174. [CrossRef]
20. Mei, B.; Zhang, J.; Shi, X.; Xi, Z.; Li, Y. Enhancement of ammonia combustion with partial fuel cracking strategy: Laminar flame propagation and kinetic modeling investigation of $NH_3/H_2/N_2$/air mixtures up to 10 atm. *Combust. Flame* **2021**, *231*, 111472. [CrossRef]
21. Mei, B.; Ma, S.; Zhang, Y.; Zhang, X.; Li, W.; Li, Y. Exploration on laminar flame propagation of ammonia and syngas mixtures up to 10 atm. *Combust. Flame* **2020**, *220*, 368–377. [CrossRef]
22. Yin, G.; Xiao, B.; Zhan, H.; Hu, E.; Huang, Z. Chemical kinetic study of ammonia with propane on combustion control and NO formation. *Combust. Flame* **2023**, *249*, 112617. [CrossRef]
23. Shrestha, K.P.; Giri, B.R.; Pelé, R.; Aljohani, K.; Brequigny, P.; Mauss, F.; Halter, F.; Huynh, L.K.; Mounaïm-Rousselle, C. A comprehensive chemical kinetic modeling and experimental study of NH_3-methanol/ethanol combustion towards net-zero CO_2 emissions. *Combust. Flame* **2025**, *274*, 113954. [CrossRef]
24. Shmakov, A.G.; Korobeinichev, O.P.; Rybitskaya, I.V.; Chernov, A.A.; Knyazkov, D.A.; Bolshova, T.A.; Konnov, A.A. Formation and Consumption of NO in H_2+O_2+N_2 Flames Doped with NO or NH_3 at Atmospheric Pressure. *Combust. Flame* **2010**, *157*, 556–565. [CrossRef]
25. Dmitriev, A.M.; Knyazkov, D.A.; Bolshova, T.A.; Tereshchenko, A.G.; Paletsky, A.A.; Shmakov, A.G.; Korobeinichev, O.P. Structure of CH_4/O_2/Ar Flames at Elevated Pressures Studied by Flame Sampling Molecular Beam Mass Spectrometry and Numerical Simulation. *Combust. Flame* **2015**, *162*, 3946–3959. [CrossRef]
26. Gerasimov, I.E.; Knyazkov, D.A.; Yakimov, S.A.; Bolshova, T.A.; Shmakov, A.G.; Korobeinichev, O.P. Structure of Atmospheric-Pressure Fuel-Rich Premixed Ethylene Flame with and without Ethanol. *Combust. Flame* **2012**, *159*, 1840–1850. [CrossRef]
27. Korobeinichev, O.P.; Shvartsberg, V.M.; Shmakov, A.G.; Knyazkov, D.A.; Rybitskaya, I.V. Inhibition of Atmospheric Lean and Rich CH_4/O_2/Ar Flames by Phosphorus-Containing Compound. *Proc. Combust. Inst.* **2007**, *31*, 2741–2748. [CrossRef]
28. Osipova, K.N.; Sarathy, S.M.; Korobeinichev, O.P.; Shmakov, A.G. Chemical Structure of Premixed Ammonia/Hydrogen Flames at Elevated Pressures. *Combust. Flame* **2022**, *246*, 112419. [CrossRef]
29. Korobeinichev, O.P.; Ilyin, S.B.; Mokrushin, V.V.; Shmakov, A.G. Destruction Chemistry of Dimethyl Methylphosphonate in H_2/O_2/Ar Flame Studied by Molecular Beam Mass Spectrometry. *Combust. Sci. Technol* **1996**, *116–117*, 51–67. [CrossRef]
30. Osipova, K.N.; Zhang, X.; Sarathy, S.M.; Korobeinichev, O.P.; Shmakov, A.G. Ammonia and Ammonia/Hydrogen Blends Oxidation in a Jet-Stirred Reactor: Experimental and Numerical Study. *Fuel* **2022**, *310*, 122202. [CrossRef]
31. Drakon, A.V.; Eremin, A.V. The Influence of Biofuels Addition on Shock-Induced Ignition and Combustion of Methane–Hydrogen Mixtures. *Fire* **2023**, *6*, 460. [CrossRef]

32. Osipova, K.N.; Korobeinichev, O.P.; Shmakov, A.G. Chemical Structure and Laminar Burning Velocity of Atmospheric Pressure Premixed Ammonia/Hydrogen Flames. *Int. J. Hydrogen Energy* **2021**, *46*, 39942–39954. [CrossRef]
33. Lee, J.H.; Kim, J.H.; Park, J.H.; Kwon, O.C. Studies on properties of laminar premixed hydrogen-added ammonia/air flames for hydrogen production. *Int. J. Hydrogen Energy* **2010**, *35*, 1054–1064. [CrossRef]
34. Lee, J.-B.; Lee, S.-I.; Kwon, O.C. Effects of ammonia substitution on hydrogen/air flame propagation and emissions. *Int. J. Hydrogen Energy* **2010**, *35*, 11332–11341. [CrossRef]
35. Li, J.; Huang, H.; Kobayashi, N.; He, Z.; Nagai, Y. Study on using hydrogen and ammonia as fuels: Combustion characteristics and NOx formation. *Int. J. Energy Res.* **2014**, *38*, 1214–1223. [CrossRef]
36. Duynslaegher, C.; Jeanmart, H.; Vandooren, J. Flame structure studies of premixed ammonia/hydrogen/oxygen/argon flames: Experimental and numerical investigation. *Proc. Combust. Inst.* **2009**, *32*, 1277–1284. [CrossRef]
37. Rocha, R.C.; Zhong, S.; Xu, L.; Bai, X.-S.; Costa, M.; Cai, X.; Kim, H.; Brackmann, C.; Li, Z.; Aldén, M. Structure and laminar flame speed of an ammonia/methane/air premixed flame under varying pressure and equivalence ratio. *Energy Fuels* **2021**, *35*, 7179–7192. [CrossRef]
38. Arunthanayothin, S.; Stagni, A.; Song, Y.; Herbinet, O.; Faravelli, T.; Battin-Leclerc, F. Ammonia-methane interaction in jet-stirred and flow reactors: An experimental and kinetic modeling study. *Proc. Combust. Inst.* **2021**, *38*, 345–353. [CrossRef]
39. He, X.; Li, M.; Shu, B.; Fernandes, R.; Moshammer, K. Exploring the effect of different reactivity promoters on the oxidation of ammonia in a jet-stirred reactor. *J. Phys. Chem. A* **2023**, *127*, 1923–1940. [CrossRef]
40. Mendiara, T.; Glarborg, P. Ammonia chemistry in oxy-fuel combustion of methane. *Combust. Flame* **2009**, *15*, 1937–1949. [CrossRef]
41. Zhou, S.; Yang, W.; Zheng, S.; Yu, S.; Tan, H.; Cui, B.; Wang, J.; Deng, S.; Wang, X. An experimental and kinetic modeling study on the low and intermediate temperatures oxidation of $NH_3/O_2/Ar$, $NH_3/H_2/O_2/Ar$, $NH_3/CO/O_2/Ar$, and $NH_3/CH_4/O_2/Ar$ mixtures in a jet-stirred reactor. *Combust. Flame* **2023**, *248*, 112529. [CrossRef]
42. Sun, Z.; Deng, Y.; Song, S.; Yang, J.; Yuan, W.; Qi, F. Experimental and kinetic modeling study of the homogeneous chemistry of NH_3 and NOx with CH_4 at the diluted conditions. *Combust. Flame* **2022**, *243*, 112015. [CrossRef]
43. Mathieu, O.; Petersen, E.L. Experimental and modeling study on the high-temperature oxidation of ammonia and related NOx chemistry. *Combust. Flame* **2015**, *162*, 554–570. [CrossRef]
44. Shu, B.; Vallabhuni, S.K.; He, X.; Issayev, G.; Moshammer, K.; Farooq, A.; Fernandes, R.X. A shock tube and modeling study on the autoignition properties of ammonia at intermediate temperatures. *Proc. Combust. Inst.* **2019**, *37*, 205–211. [CrossRef]
45. Chen, J.; Jiang, X.; Qin, X.; Huang, Z. Effect of hydrogen blending on the high temperature auto-ignition of ammonia at elevated pressure. *Fuel* **2021**, *287*, 119563. [CrossRef]
46. Dai, L.; Gersen, S.; Glarborg, P.; Levinsky, H.; Mokhov, A. Experimental and numerical analysis of the autoignition behavior of NH_3 and NH_3/H_2 mixtures at high pressure. *Combust. Flame* **2020**, *215*, 134–144. [CrossRef]
47. Pochet, M.; Dias, V.; Moreau, B.; Foucher, F.; Jeanmart, H.; Contino, F. Experimental and numerical study, under LTC conditions, of ammonia ignition delay with and without hydrogen addition. *Proc. Combust. Inst.* **2019**, *37*, 621–629. [CrossRef]
48. He, X.; Shu, B.; Nascimento, D.; Moshammer, K.; Costa, M.; Fernandes, R.X. Auto-ignition kinetics of ammonia and ammonia/hydrogen mixtures at intermediate temperatures and high pressures. *Combust. Flame* **2019**, *206*, 189–200. [CrossRef]
49. Xiao, H.; Valera-Medina, A.; Bowen, P.J. Study on premixed combustion characteristics of co-firing ammonia/methane fuels. *Energy* **2017**, *140*, 125–135. [CrossRef]
50. Xiao, H.; Lai, S.; Valera-Medina, A.; Li, J.; Liu, J.; Fu, H. Experimental and modeling study on ignition delay of ammonia/methane fuels. *Int. J. Energy Res.* **2020**, *44*, 6939–6949. [CrossRef]
51. Liu, J.; Zou, C.; Luo, J. Experimental and modeling study on the ignition delay times of ammonia/methane mixtures at high dilution and high temperatures. *Proc. Combust. Inst.* **2023**, *39*, 4399–4407. [CrossRef]
52. Dai, L.; Gersen, S.; Glarborg, P.; Mokhov, A.; Levinsky, H. Autoignition studies of NH_3/ CH_4 mixtures at high pressure. *Combust. Flame* **2020**, *218*, 19–26. [CrossRef]
53. Shu, B.; He, X.; Ramos, C.F.; Fernandes, R.X.; Costa, M. Experimental and modeling study on the auto-ignition properties of ammonia/methane mixtures at elevated pressures. *Proc. Combust. Inst.* **2021**, *38*, 261–268. [CrossRef]
54. Xiao, H.; Valera-Medina, A.; Bowen, P.J. Modeling combustion of ammonia/ hydrogen fuel blends under gas turbine conditions. *Energy Fuels* **2017**, *31*, 8631–8642. [CrossRef]
55. Somarathne, K.D.K.A.; Okafor, E.C.; Sugawara, D.; Hayakawa, A.; Kobayashi, H. Effects of OH concentration and temperature on NO emission characteristics of turbulent non-premixed CH_4/NH_3/air flames in a two-stage gas turbine like combustor at high pressure. *Proc. Combust. Inst.* **2021**, *38*, 5163–5170. [CrossRef]
56. Okafor, E.C.; Yamashita, H.; Hayakawa, A.; Somarathne, K.D.K.A.; Kudo, T.; Tsujimura, T.; Uchida, M.; Ito, S.; Kobayashi, H. Flame stability and emissions characteristics of liquid ammonia spray co-fired with methane in a single stage swirl combustor. *Fuel* **2021**, *287*, 119433. [CrossRef]

57. Giri, B.R.; Shrestha, K.P.; Mai, T.V.-T.; Giri, S.; Adil, M.; Naik, R.T.; Mauss, F.; Huynh, L.K. A Theoretical Study of NH_2 Radical Reactions with Propane and Its Kinetic Implications in NH_3-Propane Blends' Oxidation. *Energies* **2023**, *16*, 5943. [CrossRef]
58. Wang, Z.; Mei, B.; Liu, N.; Thawko, A.; Mao, X.; Zhao, H.; Glarborg, P.; Klippenstein, S.J.; Ju, Y. High pressure ammonia/methanol oxidation up to 100 atm. *Proc. Combust. Inst.* **2024**, *40*, 105489. [CrossRef]

Disclaimer/Publisher's Note: The statements, opinions and data contained in all publications are solely those of the individual author(s) and contributor(s) and not of MDPI and/or the editor(s). MDPI and/or the editor(s) disclaim responsibility for any injury to people or property resulting from any ideas, methods, instructions or products referred to in the content.